9th National Congress on Civil Engineering, 10-11 May 2016
Ferdowsi University of Mashhad, Mashhad, Iran

Nonlinear Finite Element Analysis of Solid Hybrid Precast Shear Wall under Hysteresis Loading

Fahime Shahpouri[1], Abbas Ali Tasnimi[2]

1-Master Graduate in Struct. Eng., Dept.of Civil and Envl. Eng, Tarbiat Modares University

2-Prof. in Struct. Eng., Dept.of Civil and Envl. Eng, Tarbiat Modares University

fahime.shahpouri@modares.ac.ir
tasnimi@modares.ac.ir

Abstract

Collapse prevention of structures is one of the main aim in seismic design code. Though, experiences exhibit that most of structures in sever earthquakes receive damages and residual displacements. Such permanent displacements prevents serviceability and in some cases impose repair costs. On the other hand the seismic design of self-centering system exhibits excellent performance regarding the energy dissipation, low damages and minimizing the residual displacements. The use of "hybrid" precast concrete wall structures for high seismic regions provides ample rocking mode of behavior and reduces the residual top displacements. This paper presents a three dimensional nonlinear finite element (FE) models, using ABAQUS to predict the lateral force-lateral displacement of the precast concrete shear wall specimen. The numerical analyzed carried out under both gravity and reversed-cyclic lateral loading to investigate their seismic nonlinear behavior. The obtained results indicate that the nonlinear numerical results of tested specimen are mutually correlate to the experimental results.

Keywords: Residual displacement, Hybrid shear walls, Self-centering system, Finite element analysis, Cyclic behavior.

1. INTRODUCTION

Although the use of reinforced concrete shear walls provides life-safety and collapse prevention performance, the impacts of the associated structural damage and residual drift can be significant. On the other hand, where the connections between the precast shear walls and other structural members do not have adequate strength and deformation capacity, considerable damage to precast concrete shear wall has been observed. There are two design methods for precast concrete structural systems. The first method is the emulation construction in which precast structures are detailed to emulate monolithic reinforced concrete structural systems. The second method is the jointed construction in which precast members are interconnected predominantly by dry joints.
In the non-emulative design, certain joints between precast members are allowed to deform in-elastically without significant damage. In the case of jointed construction by opening and closing certain joints between precast members, they can undergo inelastic deformations without significant damage. These locations can potentially provide inelastic deformational capacity and considerable energy dissipation [1]. The seismic performance of precast concrete structures have been improved in last decade utilizing the post-tensioned flexural reinforcement placed inside appropriate ducts. In such systems, due to lack of bond between the reinforcement and adjacent concrete, causes no damage to the concrete through bond stress transfer from the reinforcement [2&3]. Experimental and analytical studied have been carried out to investigate the behavior of unbonded precast concrete shear by a number of researchers [4-8], and it has been shown that they have excellent self-centering capability.

2. HYBRID PRECAST CONCRETE SHEAR WALLS

As shown in Figure 1, the hybrid precast concrete wall system utilizes a combination of mild steel and high-strength unbonded post-tensioning (PT) steel for lateral resistance across horizontal joints. The PT steel is

provided by multi-strand tendons placed inside un-grouted ducts to prevent bond between the steel and concrete. The tendons are connected to the structure only at end anchorages. Under the application of lateral loads into the nonlinear range, the primary mode of displacement in these walls occurs through gap opening at the horizontal joint between the base panel and the foundation. Upon unloading, the PT steel (in addition to the gravity loads) provides a restoring force to close this gap, thus reducing the residual lateral displacements of the wall. The mild steel bars crossing the horizontal joint at the base are designed to yield in tension and compression, and provide energy dissipation through the gap opening/closing behavior of the wall. A pre-determined length of these mild steel bars is unbonded by wrapping them with plastic sleeves. Both the PT steel and mild steel contribute to the lateral strength of the wall [9].

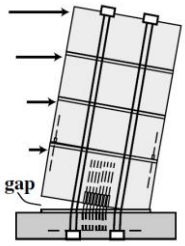

Figure 1. Displaced position of hybrid wall system [9]

3. TESTED SPECIMEN

Initial pre-test validation of the finite element analytical model was achieved by comparing the analytical results with the measured behavior of a hybrid wall tested by Smith and Kurama [10]. Specimens HW3 that named SHW in this paper, was a solid hybrid wall. Schematic drawings of SHW is shown in Figure 2. The specimen featured two wall panels: the base panel representing the 1st story of the structure and the upper panel representing the 2nd through 4th stories. Test specimen parameters required in numerical modeling are scaled wall length (L_w =2430-mm), base panel height (1450-mm) and wall thickness (t_w=159-mm). The lateral load was applied at a level of 3.66-m from the wall base, ie, the point of application of the resultant of the first mode inertial forces. An external downward axial force [325-kN] was applied at the center of the top of specimen to simulate the service-level tributary gravity loads acting on the prototype structure during an earthquake. In the hybrid system the PT steel consisted of two bundles of strand located 229-mm north and south from the wall centerline. Each PT steel bundle included three 13-mm diameter strands (design ultimate strength=1862 MPa) with an unbonded length from the top of the wall to the bottom of the foundation beam of 5.48-m. The average initial tendon stress, calculated from the measured individual strand forces prior to the application of the lateral load, was $f_{pi}=0.54f_{pu}$. The mild steel reinforcement crossing the base joint in the hybrid specimen consisted of 4Φ19 bars (measured yield strength=448 MPa), with one pair of bars located 152-mm north and south from the wall centerline and the other pair 76-mm north and south from the centerline. Across the panel-to-panel joint, only 2Φ19 bars were used, with one bar located 102-mm from each end of the wall. This reinforcement was designed not to yield so as to limit any gap opening or slip along the panel-to-panel joint.

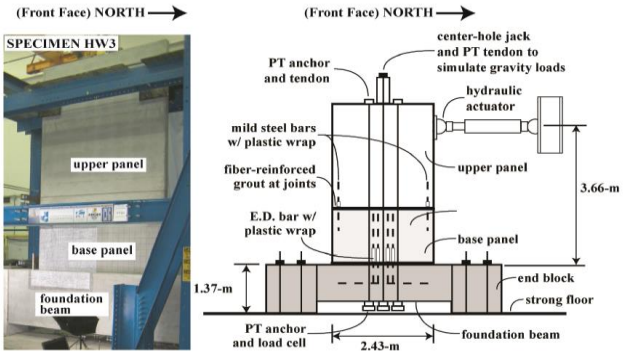

Figure 2. Photograph and schematic of SHW [10]

3. ANALYTICAL MODEL

This paper presents a three dimensional nonlinear finite element (FE) models, using ABAQUS/Standard [11] to predict the lateral force-lateral displacement of the precast concrete shear wall specimen.

3.1. MATERIAL PROPERTIES

The stress-strain relationships for the PT steel, energy dissipating mild steel (ED steel) and confinement steel bars were modeled using a multiple-point approximation of the measured monotonic material test data, as shown in Figure 3. Each material model included "elastic" and "plastic" regions.

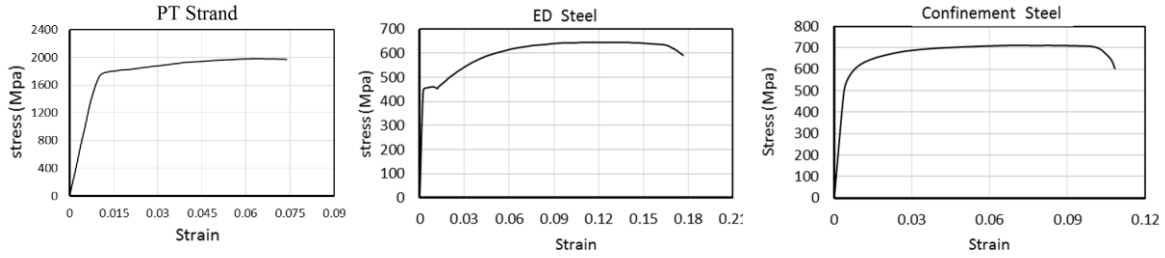

Figure 3. Material behavior: PT strand, E.D. steel and confinement steel

The concrete damaged plasticity model was used to define the behavior of the concrete. The plastic-damage model in ABAQUS is based on the models proposed by Lubliner et al. [12] and by Lee and Fenves [13]. Five parameters are required to define the yield surface, flow potential, and viscosity parameters for the concrete damaged plasticity constitutive model: the dilation angle in degrees, the flow potential eccentricity, the ratio of initial equibiaxial compressive yield stress to initial uniaxial compressive yield stress, the ratio of the second stress invariant on the tensile meridian to that on the compressive meridian, and the viscosity parameter that defines visco-plastic regularization. The aforementioned parameters were set to 1, 0.1, 1.16, 0.667, and 0, respectively. If Eo is the initial (undamaged) elastic stiffness of the material, the stress-strain relations under uniaxial tension and compression loading given by equations 1and 2 respectively.

$$\sigma_t = (1 - d_t)E_0(\varepsilon_t - \tilde{\varepsilon}_t^{pl}) \quad (1)$$

$$\sigma_c = (1 - d_c)E_0(\varepsilon_c - \tilde{\varepsilon}_c^{pl}) \quad (2)$$

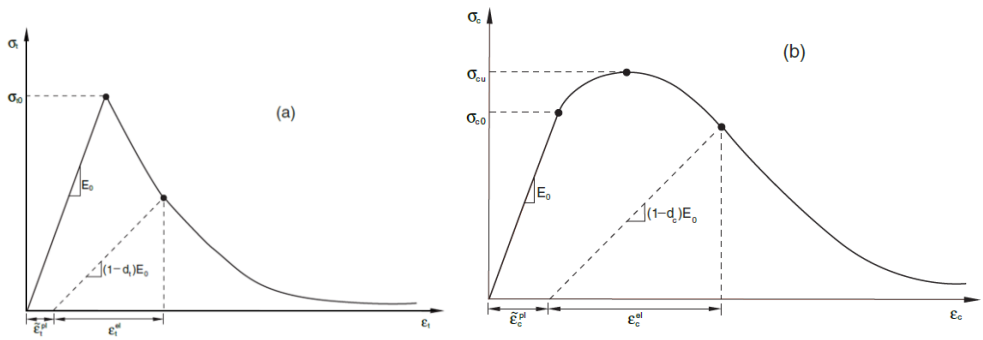

Figure 4. Response of concrete to uniaxial loading in (a) tension and (b) compression

Under uniaxial cyclic loading conditions the degradation mechanisms are quite complex, involving the opening and closing of previously formed micro-cracks, as well as their interaction. Experimentally, it was observed that there was some recovery of the elastic stiffness as the load changed sign during a uniaxial cyclic test. The stiffness recovery effect, also known as the "unilateral effect," is an important aspect of the concrete behavior under cyclic loading. The effect is usually more pronounced as the load changes from tension to compression, causing tensile cracks to close, which results in the recovery of the compressive stiffness. The concrete damaged plasticity model assumes that the reduction of the elastic modulus is given in terms of a scalar degradation variable d.

$$E = (1-d)E_0 \quad (3)$$

In equation 3, E_0 is the initial (undamaged) modulus of the material. This expression holds both in the tensile ($\sigma_{11} > 0$) and compressive ($\sigma_{11} < 0$) sides of the cycle. The stiffness reduction variable, d, is a function of the stress state and the uniaxial damage variables, d_c and d_t. For the uniaxial cyclic conditions, Abaqus assumes equations 4.

$$(1-d) = (1-s_t d_c)(1-s_c d_t), 0 \le s_t, s_c \le 1 \quad (4)$$

where s_t and s_c are functions of the stress state that are introduced to represent stiffness recovery effects associated with stress reversals. Figure 5 shows the example where the load changes from tension to compression. Assume that there was no previous compressive damage (crushing) in the material.

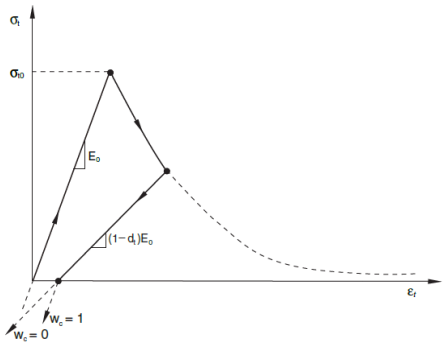

Figure 5. Illustration of the effect of the compression stiffness recovery parameter w_c

The evolution equations for the hardening variables must be extended for the general multiaxial conditions. Based on Lee and Fenves [13] we assume that the equivalent plastic strain rates are evaluated according to the expressions 5 and 6.

$$\dot{\tilde{\varepsilon}}_t^{pl} \overset{\text{def}}{=} r(\hat{\bar{\sigma}})\dot{\hat{\varepsilon}}_{max}^{pl} \quad (5)$$

$$\dot{\tilde{\varepsilon}}_c^{pl} \overset{\text{def}}{=} -(1-r(\hat{\bar{\sigma}}))\dot{\hat{\varepsilon}}_{max}^{pl} \quad (6)$$

where $\dot{\hat{\varepsilon}}_{max}^{pl}$ and $\dot{\hat{\varepsilon}}_{max}^{pl}$ are, respectively, the maximum and minimum eigenvalues of the plastic strain rate tensor $\dot{\varepsilon}_{pl}$ and

$$r(\hat{\bar{\sigma}}) \overset{\text{def}}{=} \frac{\sum_{i=1}^{3}\langle\hat{\bar{\sigma}}_i\rangle}{\sum_{i=1}^{3}|\hat{\bar{\sigma}}_i|};\ 0 \le r(\hat{\bar{\sigma}}) \le 1 \quad (7)$$

The plastic-damage concrete model uses a yield condition based on the yield function proposed by Lubliner et al. [12] and incorporates the modifications proposed by Lee and Fenves [13] to account for different evolution of strength under tension and compression. In terms of effective stresses the yield function takes the form:

$$F(\bar{\sigma}, \tilde{\varepsilon}^{pl}) = \frac{1}{1-\alpha}\left(\bar{q} - 3\alpha\bar{p} + \beta(\tilde{\varepsilon}^{pl})\langle\hat{\bar{\sigma}}_{max}\rangle - \gamma\langle\hat{\bar{\sigma}}_{max}\rangle\right) - \bar{\sigma}_c(\tilde{\varepsilon}_c^{pl}) \le 0 \quad (8)$$

Where α and γ are dimensionless material constants, $\bar{p}$ is the effective hydrostatic pressure, $\bar{q}$ is the Mises equivalent effective stress and $\bar{S}$ is the deviatoric part of the effective stress tensor $\bar{\sigma}$ given by equations 9, 10 and 11 respectively. $\hat{\bar{\sigma}}_{max}$ is the algebraically maximum eigenvalue of $\bar{\sigma}$.

$$\bar{p} = -\frac{1}{3}\,\bar{\sigma} : \mathrm{I} \quad (9)$$

$$\bar{q} = \sqrt{\frac{3}{2}\,\bar{S} : \bar{S}} \quad (10)$$

$$\bar{S} = \bar{p}\mathrm{I} + \bar{\sigma} \quad (11)$$

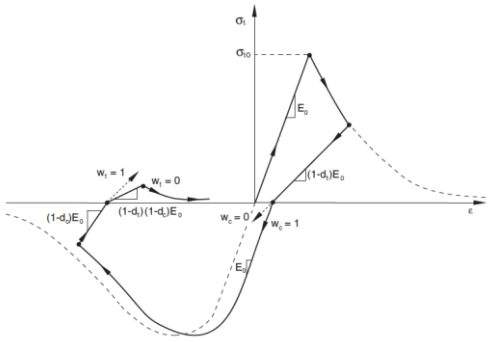

Figure 6. Uniaxial load cycle (tension-compression-tension) assuming default values for the stiffness recovery factors: $w_t = 0$ and $w_c = 1$

Figure 7 illustrates the typical yield surfaces in the deviatoric plane and for the case of plane-stress conditions.

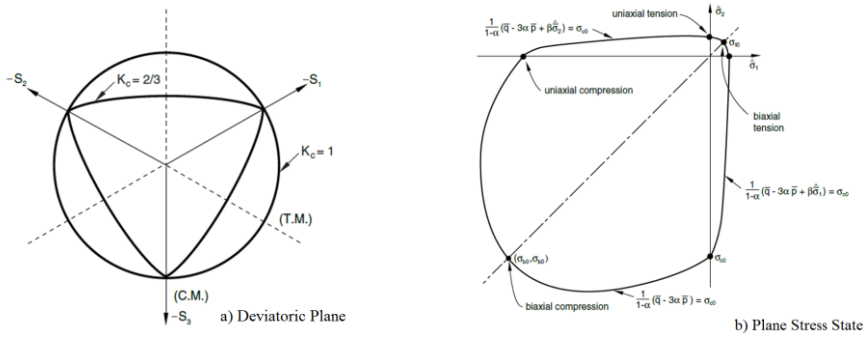

Figure 7. Yield surfaces in the deviatoric plane and plane stress state

In the present numerical analysis the concrete behavior in compression and tension was modeled utilizing a multiple-point approximation of the material stress-strain relationships containing the "elastic" and "plastic" states. The unconfined concrete stress-strain behavior was created based on the measured concrete strength and initial stiffness using the relationship from Maekawa [14]. For confined concrete, the confinement reinforcement was modeled explicitly in the finite element analysis. Any additional concrete confinement effects developing due to the transverse stresses in the finite element model were considered.

3.2. FEATURES OF NUMERICAL MODELING

The finite element models were created for the 0.4 scaled test specimen and utilized the following features:

1- To represent the end anchorages of the PT tendons, steel anchorage plates were modeled and connected to the foundation and upper panel concrete elements and for modeling the anchorage ends of the PT tendons these truss elements connected to the steel plate elements using "tie constraints."

2- The initial post-tensioning stresses in the PT steel were simulated by placing an initial tension force in the truss elements for the tendons.

3- The truss elements modeling the energy dissipating mild steel bars across the base joint were partitioned into bonded and unbonded regions. In the bonded regions of the bars (located in both the base panel and the foundation), the truss elements were embedded within the concrete elements using embedded region constraints. The elements in the unbonded regions were not constrained, thereby allowing a uniform strain distribution to form over the unbonded length. The bonded and unbonded portions of the mild steel reinforcement across the upper joint were modeled in the same manner.

4- The bonded mild steel reinforcement contained within the wall panels and the foundation beam was modeled explicitly.

5- The wall model included three dimensional eight-node stress/displacement solid elements for the wall panels and the foundation fixtures. Three dimensional stress/displacement truss elements were used for the PT steel, energy dissipating mild steel crossing the base joint, and mild steel reinforcement crossing the upper joint.

6- The biggest "crack" in a hybrid precast concrete wall is the gap that forms at the base joint, which is appropriately included in the model by using contact surfaces at this joint. To allow for gap opening at the horizontal joints, the model incorporated "hard contact" surfaces at these joints. For tangential components of the contact surfaces, coefficients of frictions of 0.5 were selected for concrete/concrete.

7- To simulate the boundary condition of the foundation, the U_x, U_y, and U_z degrees of freedom (DOF) were constrained for all the nodes at the bottom surface of the foundation.

4. PRETENSIONING

As described previously, the initial Stresses in the PT steel (after all short term and long term losses but before Lateral displacements of the wall) were simulated by placing an initial tension force in the relevant truss elements (Figure 8). From Figure 8 it is clear that the stresses were concentrated at end blocks of PT anchors, whereas they distributed uniformly (almost 3 MPa) as distant from the anchorages.

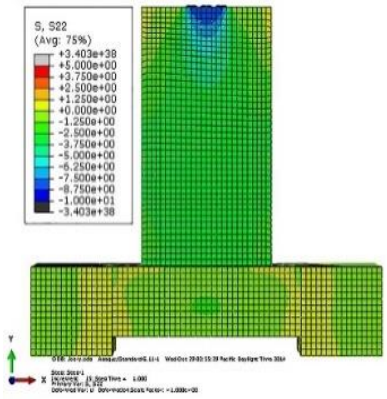

Figure 8. Stress distribution due to prestressing

5. LATERAL LOAD

Figure 9 shows the reversed-cyclic lateral displacement history used in the numerical modeling of the wall specimen with one cycle at each displacement increment. The wall drift, Δ_w was measured as the relative lateral displacement of the wall between the lateral load location and the foundation divided by the height to the lateral load.

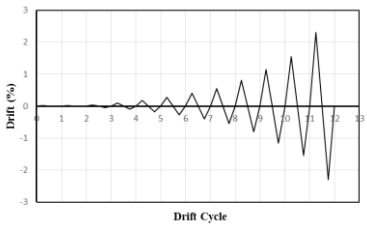

Figure 9. Wall drift history used for numerical analysis

6. RESULT

The most important results obtained in numerical analysis are discussed in the following. In addition to the hysteresis behavior (overall behavior) represented by lateral force versus lateral displacement, other major parameters namely energy distributed (ED) by steel bars and PT steel, gap opening and displacement at wall end are also discussed.

6.1. LATERAL LOAD VERSUS DISPLACEMENT BEHAVIOR

Figure 9 shows the measured base shear force versus wall drift and corresponding analytical behavior predicted by the finite element model for specimen SHW. The wall behaved in a reasonably symmetrical manner in the positive and negative directions, and exhibited excellent recentering and considerable energy dissipation. While crushing of the confined concrete was observed at the wall toes, the total strength loss from the overall peak base shear force during the test to the peak force during the final cycle was 19.9% and 13.8% in the positive and negative directions, respectively.

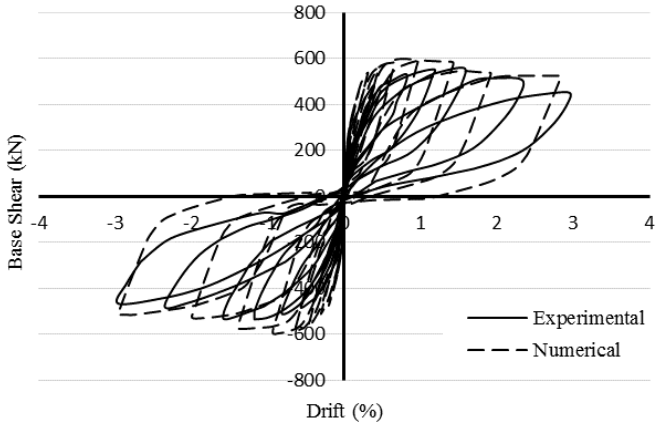

Figure 9. Measured and numerical base shear force versus wall drift behaviors

6.2. ED BAR BEHAVIOR

As described, the ED bars had plastic-wrapped unbonded lengths to limit the tensile steel strains, while also allowing significant yielding of the bars as the walls were displaced. Because the mild steel bars crossing the base joint serve as the main energy dissipater for the wall, it is essential for these bars to yield well before the design-level drift (Δ_{wm}=2.3%) but not fracture before the validation-level drift (Δ_{wd}=0.7%). Figure 9 shows the measured and numerically evaluated steel strains for the north intermediate ED bar in Specimen SHW. Due to gauge failure, measurements could only be taken up to a maximum strain of 0.015 cm/cm at Δ_w=1.15%.

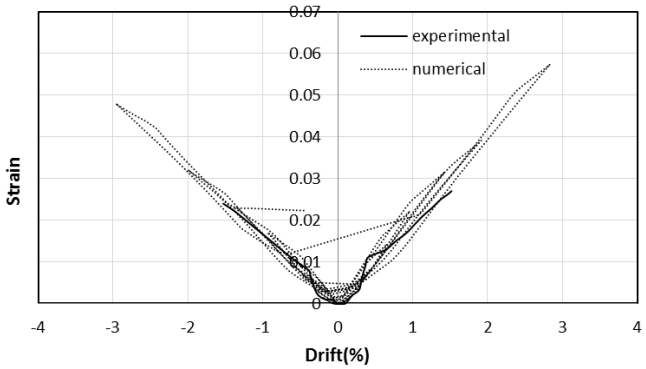

Figure 9. Measured and numerical E.D steel bar strains

6.3. PT STEEL BEHAVIOR

Figure 10 shows the numerical PT stress for specimen SHW in the north and south PT tendons. The PT tendons remained essentially linear-elastic until Δ_w=1.55%, which was possible because the strands were unbonded over their length. Losses in the PT stresses, which occurred primarily because of a small amount of nonlinear behavior in the strand-anchorage system, can be seen during the large displacement cycles and are clearly visible upon unloading from the final drift cycle.

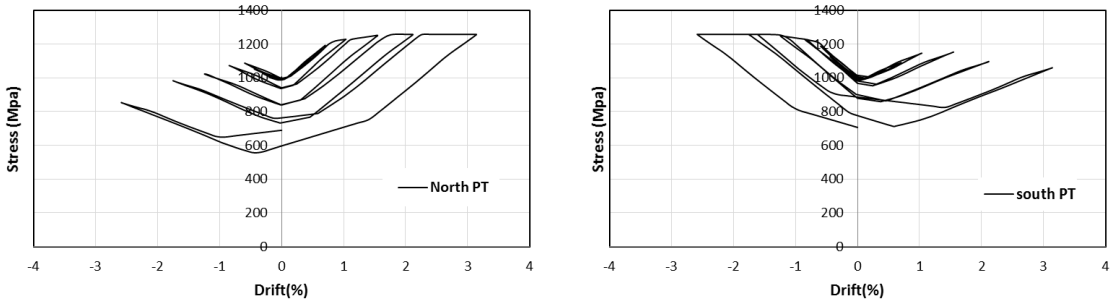

Figure 10. Numerical PT steel tendon stresses

6.5. GAP OPENING

Consistent with the design expectations, specimen have a significant gap at the base joint while the gap opening at the upper joint was negligible. Figure 11 shows the numerical, maximum gap opening displacements at the base joint at the extreme north and south ends of specimens SHW.

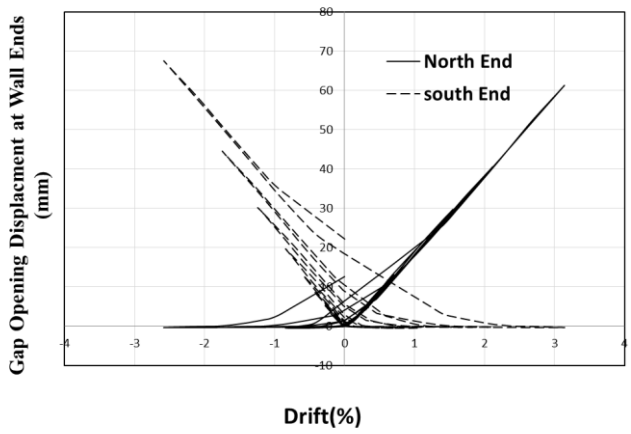

Figure 11. Numerical base joint gap opening displacements at wall ends

7. CONCLUSIONS

This paper presents the numerical modeling of a tested 0.40-scale hybrid precast concrete wall specimen. Numerical modeling considers all the details of tested specimen and the nonlinear behavior of all materials used. The obtained results indicate that the nonlinear numerical results of tested specimen correlate with the experimental results. Based on the cited experimental results and the results predicted by the numerical models developed in this study, the following conclusions can be made:

1- The ABAQUS modeling techniques developed here can be used to predict the lateral load-drift response of unbonded, post-tensioned solid hybrid precast concrete shear walls.
2- Pretensioning is the main factor that providing restoring force were simulated by placing an initial tension force in the PT elements.
3- The tendons has significant effect on the lateral stiffness capacities.
4- The mild steel bars crossing the base joint has significant effect on the energy dissipation capacities.
5- The numerical models matched the measured base shear force versus wall drift reasonably well.
6- Consistent with the experimental result, numerical base shear force versus wall drift was symmetrical and exhibited excellent recentering and considerable energy dissipation.
7- The PT tendons remained essentially linear-elastic until $\Delta w=1.55\%$.

8. REFERENCES

1. Schultz, A., Cheok, G., and Magana, R. [1998] ‘‘Performance of precast concrete shear walls’’, Proc. 6th U.S. National Conference on Earth. Engineering, EERI, Oakland, CA, 1998.
2. Cheok, G. S., Stone, W. C., and Lew, H. S. [1993] ‘‘Seismic performance behavior of precast concrete beam-column joints,’’ Proc., Symposium on Structural Engineering in National Hazard Mit., ASCE, Reston, VA, pp. 83–88.
3. Priestley, M. J. N. and Tao, J. R. T. [1993] ‘‘Seismic response of precast prestressed concrete frames with partially debonded tendons,’’ PCI Journal 38(1), 58–69.
4. Kurama, Y. [2002] ‘‘Hybrid post-tensioned precast concrete walls for use in seismic regions,’’PCI Journal47(5),36–59.
5. Kurama,Y., Sause,R., Pessiki,S., Lu,L.-W., and El-Sheikh,M., [1997], ‘‘Seismic design and response evaluation of unbonded post-tensioned precast concrete walls,’’ Res. Rep. No. EQ-97-01, Department of Civil and Environmental Engineering, Lehigh University, 184 pp.
6. Kurama, Y., Pessiki, S., Sause, R., Lu, L.-W., and El-Sheikh. M.[1996] ‘‘Analytical modeling and lateral load behavior of unbonded post-tensioned precast concrete Walls,’’ Rep. No. EQ-96-02, Department of Civil and Environmental Engineering, Lehigh University, Bethlehem, PA, 191 pp.
7. Schultz, A., Cheok, G., and Magana, R. [1998] ‘‘Performance of precast concrete shear walls’’, Proc. 6th U.S. National Conference on Earth. Engineering, EERI, Oakland, CA, 1998.
8. Holden, T.J. [2001] ‘‘A comparison of the seismic performance of precast wall construction: emulation and hybrid approaches,’’ Res. Rep. 2001–04, University of Canterbury, Christchurch, New Zealand. International Building Code[2006]. International Code Committee, Whittier, CA.
9. Smith, B. J., Kurama, Y. C., & McGinnis, M. J. (2010).”"Design and measured behavior of a hybrid precast concrete wall specimen for seismic regions”, Journal of Structural Engineering, 137(10), 1052-1062.
10. Smith, B. J., Kurama, Y. C., & McGinnis, M. J. (2013). “Behavior of Precast Concrete Shear Walls for Seismic Regions: Comparison of Hybrid and Emulative Specimens”, Journal of Structural Engineering, 139(11), 1917-1927.
11. Hibbitt, Karlsson, and Sorenson, “ABAQUS User's Manual - Version 6.11.1,” Hibbitt, Karlsson & Sorenson, Inc., 2011.
12. Lubliner, J., Oliver, J., Oller, S., & Onate, E. (1989). A plastic-damage model for concrete. International Journal of solids and structures, 25(3), 299-326.
13. Lee. J., Fenves. G.L, “Plastic-Damage Model for Cyclic Loading of Concrete Structure,” Jornal of Engineering Mechanics, 1998;124(8):892-900
14. Maekawa. K., Pimanmar, A. and Okamura. H., 2003. “Non-Linear Mechanics of Reinforced Concrete”, Spon Press, Taylor and francis.